THE JOURNAL OF PHYSICAL CHEMISTRY B

Article

pubs.acs.org/JPCB

Photoinduced Excited State Electron Transfer at Liquid/Liquid Interfaces

Jason K. Cooper and Ilan Benjamin*

Department of Chemistry and Biochemistry University of California Santa Cruz, California 95064, United States

Supporting Information

ABSTRACT: Several aspects of the photoinduced electron transfer (ET) reaction between coumarin 314 (C314) and *N*,*N*-dimethylaniline (DMA) at the water/DMA interface are investigated by molecular dynamics simulations. New DMA and water/DMA potential energy surfaces are developed and used to characterize the neat water/DMA interface. The adsorption free energy, the rotational dynamics, and the solvation dynamics of C314 at the liquid/liquid interface are investigated and are generally in reasonable agreement with available experimental data. The solvent-free energy curves for the ET reaction between excited C314 and DMA molecules are calculated and compared with those calculated for a simple point charge model of the solute. It is found that the reorganization free energy is very small when the full molecular description of the solute is taken into account. An estimate of the ET rate constant is in reasonable agreement with experiment. Our calculations suggest that the polarity of the surface "reported" by the solute, as reflected by solvation dynamics and the reorganization free energy, is strongly solute-dependent.

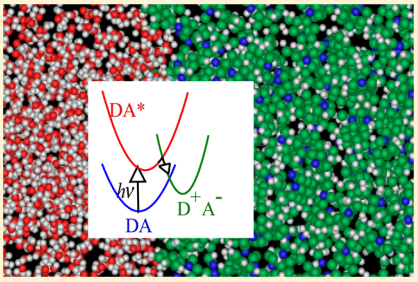

I. INTRODUCTION

Understanding electron transfer (ET) at the interface between two immiscible electrolyte solutions (IES) is of fundamental importance in electrochemistry,[1−7] solar energy conversion and "artificial photosynthesis",[8,9] and phase transfer catalysis[10−12] and may also be relevant to understanding biological processes at membrane interfaces and in DNA environments.[13] The experimental study of ET at IES has a long history,[2] but up until recently, measurements of electron transfer rates have mainly utilized conventional electrochemical methods, where the interface was under potentiostatic control.[2,14] These measurements suffer from several drawbacks, including an inability to clearly distinguish between electron and ion transfer, a narrow potential window, distortion due to charging current, and large resistivity of the organic phase. These drawbacks limit the number of experimental systems that can be studied and, thus, very few reliable rate constants have been reported. In recent years, there has been a surge in experimental activity due to the employment of new methods in which the above drawbacks can be minimized or controlled. This includes scanning electrochemical microscopy (SECM),[15−26] thin-layer cyclic voltammetry,[27,28] and spectro-electrochemical methods (some utilizing recent advances in nonlinear optics).[5,6,29−44]

In the SECM technique, the ability to widen the potential window significantly (because there is typically no need for supporting electrolytes in the two phases) increases the range of the driving force ($-\Delta G_{rxn}$) for the ET at IES and has thus recently enabled the observation of the Marcus-inverted region and a reliable determination of the reorganization free energy.[16,19,25,45,46]

Spectroelectrochemical methods have been used in recent years to study fast photoinduced electron transfer (PET) at the liquid/liquid (L/L) interface.[32−36,47] Of particular importance is extending to the L/L interface the idea of using a solvent, such as *N*,*N*-dimethylaniline (DMA) as an electron donor.[37,48−51] The advantage of this approach is that complications due to ion transfer across the interface and to diffusion are removed. Recently, several studies of PET between coumarin dyes and electron-donating solvents in micelles, reverse micelles, at the surface of proteins and in nanocavities have demonstrated ultrafast electron transfer that is faster than solvation due to the close proximity of the redox pair. These experiments have provided additional examples of the existence of the Marcus-inverted region at liquid interfacial systems.[38−44,52]

There have only been a few theoretical studies of ET at L/L interfaces. Most have utilized continuum electrostatic models to compute the reorganization free energy and the activation free energy.[1,53,54] A theory of the rate constant for ET in the case when one reactant is in the aqueous phase and the other in the organic phase was developed by Marcus[55,56] and applied to the reaction between the $Fe(CN)_6^{4-/3-}$ couple in water and the $Lu(PC)_2^{+/2+}$ (hexacyanoferrate-lutetium biphthalocyanine) couple in 1,2-dichloroethane (DCE). The theory has also been applied to ET at the solution−semiconductor interface.[57,58] Tavernier et al. used a continuum electrostatic model to calculate the reorganization free energy and the reaction free energy for a redox pair at the surface of model spherical micelles.[59] Recently, a phenomenological thermodynamic

Special Issue: James L. Skinner Festschrift

Received: September 24, 2013
Revised: December 18, 2013

   dx.doi.org/10.1021/jp409541u | *J. Phys. Chem. B* XXXX, XXX, XXX−XXX

approach based on partial desolvation of ions at interfaces has been used to estimate the activation free energy for two different reactions, assuming either a sharp boundary model[60] or a diffuse model for the interface structure.[61]

We used molecular dynamics simulations and the umbrella biasing technique developed by Warshel[62] to calculate the reorganization free energy for ET at a model L/L interface[63] and at the water/DCE interface[64] in order to assess the accuracy of the continuum electrostatic model. While the agreement was found to be reasonable, the continuum model is quite sensitive to the value of the ion cavity size and the location of the redox couple at the interface, neither of which is typically known.

In this paper we examine theoretically several aspects of the photoinduced electron transfer reaction at the water/DMA interface studied by Eisenthal and co-workers using pump-(nonlinear response) probe experiments.[37,51] In the experiment schematically described in Figure 1, a 423 nm photon excites coumarin 314 (C314) adsorbed at the water/DMA interface. The electron transfer from an interfacial DMA molecule to the excited state coumarin (C314*) produces an interfacial radical ion pair ($DMA^{+\bullet}/C314^{-\bullet}$), which may recombine to form the ground state molecules by a back electron transfer (BET) or remain as a contact or solvent-separated ion pair. The ET reaction was first monitored[37] by following the Second Harmonic Generation (SHG) probe signal resonant with the C314 $S_0 \rightarrow S_1$ transition giving a forward ET time constant of 14 ± 2 ps or by following the SHG signal resonant with an electronic transition in the DMA radical cation giving a time constant of 16 ± 3 ps. More recently,[51] an experiment using a Sum Frequency Generation (SFG) probe resonant with the C=O vibrational frequency in C314 gave a similar time constant of 16 ± 2 ps. This time constant represents an ET rate that is (surprisingly) twice as fast as the reaction of C153 in bulk DMA (expected to be similar to that of the rate for C314). This was attributed[51] to the water/DMA interface being less polar than bulk DMA, because the reorganization free energy and, correspondingly, the activation free energy should be smaller in a less polar medium. The lower polarity of the interface relative to bulk DMA was suggested by the observation that the surface SHG spectrum of C314 is shifted to the blue relative to the UV spectrum of C314 in bulk DMA and in bulk water.[51] This is a counterintuitive result, as typically the polarity of the interface tends to lie between the polarity of two bulk phases.[65,66]

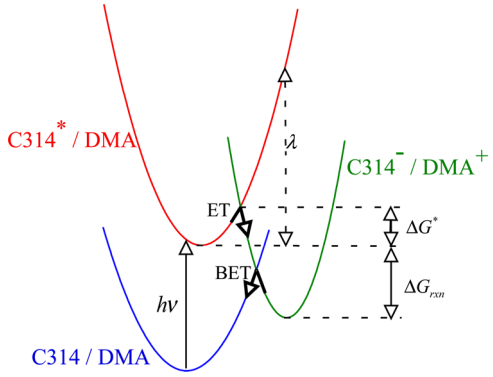

Figure 1. Schematic representation of the states involved in the electron transfer (ET) and back electron transfer (BET) processes. A 423 nm photon excites coumarin 314 (C314) adsorbed at the water/*N*,*N*-dimethylaniline (DMA) interface. The electron transfer produces the interfacial ion pair, which may recombine to give the ground state molecules. λ is the reorganization free energy for the reactants' state.

This experiment raises several important questions that have yet to be addressed for ET at liquids interfaces. To facilitate this discussion, it is useful to have in mind the following simple expression for the ET rate constant, which is an effective first-order formula applicable to the photoinduced experiment that measures the recovery of the SHG signal (or the fluorescence decay rate in the bulk experiments):[67−70]

$$k_{ET} = \frac{k_{NA}}{1+\kappa}, \quad k_{NA} = \frac{2\pi}{\hbar}\frac{V_{el}^2}{\sqrt{4\pi\lambda_s k_B T}} e^{-\Delta G^*/k_B T}, \quad \kappa = \frac{4\pi V_{el}^2 \tau_L}{\hbar \lambda_s} \tag{1}$$

where k_{NA} is the nonadiabatic rate constant, κ is the adiabaticity parameter, V_{el} the electronic coupling between the donor and acceptor, τ_L the solvent longitudinal relaxation time,[71] λ_s the solvent reorganization free energy, T the temperature, ΔG^* the activation free energy, k_B the Boltzmann constant, and $\hbar$ Planck constant. When the adiabaticity parameter is much less than 1 (weak coupling), the ET is nonadiabatic, and when $\kappa \gg 1$, the ET is adiabatic and the rate is inversely proportional to the solvent relaxation time:

$$k_{ET}(\text{adiabatic}) \approx \sqrt{\frac{\lambda_s}{16\pi k_B T}} \frac{1}{\tau_L} e^{-\Delta G^*/k_B T} \tag{2}$$

i. Role of Surface Structure. Experiments[72,73] and a large body of computer simulations[74−77] suggest that the L/L interface is rough and that this roughness increases in the presence of adsorbed ionic species.[78−80] On the other hand, the electronic coupling is strongly dependent on the distance between the donor and acceptor and on their relative orientation. For example, in a detailed study of V_{el} for electron transfer between C152 and DMA in bulk DMA, values ranging from 1 to 800 cm^{-1} were found even among DMA molecules within the first hydration shell of the solute.[49] Clearly the adiabaticity parameter κ in eq 1 will depend on the relative location, orientation and conformation of the donors and acceptor molecules. These suggest that at the L/L interface, κ will depend on the local interface fluctuations.

ii. Role of Surface Polarity. In the SFG experiment by Rao et al.,[51] the faster ET rate at the interface than in Bulk DMA was correlated with lower polarity of the interface. In most water/liquid interfaces, surface polarity is close to the average of the two bulk phases and higher than that of the bulk organic phase.[65,81] In the case of the water/octanol interface, the lower polarity of the interface than of bulk octanol was attributed to a hydrocarbon layer produced by a monolayer of octanol molecules oriented at the interface.[82] What is the molecular basis for the low polarity of the water/DMA interface?

iii. Reorganization Free Energy When the Solvent Is the Electron Donor. The continuum models and the molecular dynamics calculations of λ_s reported to date involve donor and acceptor solute molecules at the interface between two liquids. In the experiments of Eisenthal and co-workers, the donor molecule is one of the organic solvent molecules, while the acceptor is a coumarin dye at the interface. Clearly the computational methodology needs to be modified to take into account that solvent polarization fluctuations around a number of potential donors (that also act as part of the solvent) must be

dx.doi.org/10.1021/jp409541u | J. Phys. Chem. B XXXX, XXX, XXX−XXX

analyzed. This also presents a challenge in the molecular interpretation of λ_s.

iv. Solvation Dynamics. Solvation dynamics play an important role in fast ET reactions, and it could also be the controlling factor. In the experiments mentioned above by Eisenthal and co-workers, the fast subpicosecond component of the SHG or SFG signal recovery was attributed to the solvation dynamics of the excited state dye at the interface. In addition, important contributions from solvation dynamics may affect the fate of the ion-pair following the ET process. While solvation dynamics at the liquid/liquid interface have been studied by us in general for some model L/L interfaces,[83] an analysis of the above experiment is necessary.

It should be noted that, although DMA's solubility in water is quite small, some small fraction of interfacial DMA molecules may be protonated. Our model does not take this into consideration. However, using DMA's pK_a value of 5.15, we estimate a negligible concentration of DMA^+OH^- relative to the C314 surface concentration.

Below, we describe a detailed molecular model of the system that enables us to address, to some degree, the above issues.

II. SYSTEMS AND METHODS

1. Systems and Potentials. The main system under study includes a single coumarin (C314) molecule adsorbed at the water/DMA liquid/liquid interface (see Figure 2). The

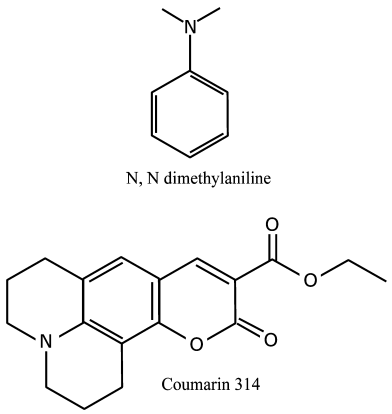

Figure 2. Chemical structures of DMA and coumarin 314 molecules.

simulation box has a cross section of 33.6 Å × 33.6 Å and includes 950 water and 252 DMA molecules. Additional benchmark calculations for testing and comparisons were done with the C314 in the bulk of the two liquids and for a model diatomic solute located at the water/DMA interface and in the bulk of the two liquids. To investigate the different processes described in Figure 1 we require potential energy surfaces for DMA, DMA^+, C314, C314*, and $C314^-$. For simplicity, we model all these molecules using a fully flexible all-atoms intramolecular potential with stretching, bending, torsion and improper torsion parameters taken from the OPLS all-atoms forcefield.[84] However, for the water intramolecular potential we use a power series function fitted to spectroscopic data.[85] The intermolecular part of the potential energy is represented by a sum of atom-based Lennard-Jones plus Coulomb terms for all the molecules in the system:

$$u_{ij}(r) = 4\varepsilon_{ij}\left[\left(\frac{\sigma_{ij}}{r}\right)^{12} - \left(\frac{\sigma_{ij}}{r}\right)^{6}\right] + \frac{q_i q_j}{4\pi r\varepsilon_0} \quad (3)$$

where "i" and "j" denote atoms (not in the same molecule) separated by a distance r. The Lennard-Jones parameters σ_{ij} and ε_{ij} for the interaction between atom types "i" and "j" are determined from the "self" terms using the standard (Lorentz–Berthelot) mixing rules:[86] $\sigma_{ij} = (\sigma_{ii} + \sigma_{jj})/2$, $\varepsilon_{ij} = (\varepsilon_{ii}\varepsilon_{jj})^{1/2}$. For simplicity, we choose the Lennard-Jones parameters σ_{ii} and ε_{ii} for atom type "i" to be independent of the electronic state of the molecules. Thus, only the atomic charge distribution distinguishes between the different electronic states. The values of the Lennard-Jones parameters and partial charges for water are those of the simple point charge model (SPC),[87] and for C314 and C314*, the parameters are taken from the work of Pantano and Laria.[88] The Lennard-Jones parameters for DMA are taken from the OPLS force field. The charge distributions on DMA, DMA^+, and $C314^-$ were determined using Gaussian09.[89] For $C314^-$, the structure was optimized with B3LYP/6-31++G(d,p). DMA and DMA^+ were optimized with MP2/6-31+G(d,p). Single point calculations for DMA/DMA^+ and C314/$C314^-$ were performed with the B2PLYP[90] functional and the cc-pvtz and 6-311++(3df,2p) basis set, respectively. Atomic charges were calculated with ChelpG.[91] All these parameters are given in the Supporting Information.

It is well-known that properties of the interface region reported by a probe may depend on the probe size, charge distribution, and other structural motifs.[66] In order to determine the effect of the probe charge distribution on the polarity of the interface and the reorganization free energy, charge transfer test calculations with the C314*/DMA pair replaced by a pair of neural atoms (DA) and the $C314^-/DMA^+$ pair replaced by the charged pair (D^+A^-) were also carried out. In these calculations, the atom pair was held at the fixed distance of 2, 3 and 4 Å, and the Lennard-Jones parameters were selected to be equal: $\varepsilon_A = \varepsilon_D = 0.2$ kcal/mol; $\sigma_A = \sigma_B = 3$ Å.

2. Methodology and Simulation Details. The following calculations have been carried out:

(a). Characterization of the Structure of the Neat Water/DMA Interface. This is accomplished with a fixed temperature 20 ns trajectory of the liquid/liquid interface with no solute molecules present.

(b). Orientational Distribution, Rotational Dynamics, and Adsorption Free Energy of C314 at the Interface. The free energy calculations are done by computing the center of mass distribution of the C314 in a series of overlapping 3 Å wide "windows" in the direction of the interface normal. In each window, "n", the free energy profile is determined from a 5 ns trajectory according to $A(z) = -RT\ \ln P_n(z)$, and these are combined together[92−94] to obtain the profile for transporting C314 from bulk water to bulk DMA.

(c). Equilibrium and Nonequilibrium Solvation Dynamics Calculations Following the Transition C314 → C314 in Bulk Solvents and at the Water/DMA Interface.* At each nuclear configuration, we define the energy gap coordinate by $\Delta E(\mathbf{r}) = E_{ex} - E_{gr}$, where E_{ex} and E_{gr} are the total excited and ground state energies of the system. The normalized equilibrium correlation function[66,95−97]

$$C_\nu(t) = \frac{\langle \delta E(t)\delta E(0)\rangle_\nu}{\langle \delta E(0)\delta E(0)\rangle_\nu}, \quad \delta E(t) = \Delta E(t) - \langle \Delta E(t)\rangle_\nu \quad (4)$$

where $\langle\ \rangle_\nu$ denotes the equilibrium ensemble averages with the dynamics governed by the Hamiltonian H_ν (n = gr or ex), is computed using a 20 ns trajectory, where the C314 or the

dx.doi.org/10.1021/jp409541u | J. Phys. Chem. B XXXX, XXX, XXX−XXX

C314* are located either in bulk solvents or at the interface. Nonequilibrium calculations use an ensemble of 480 independent configurations, where the solvents are equilibrated to ground state C314. The charge distribution is switched to that of C314*, and each configuration is followed for 50 ps. The nonequilibrium correlation function is computed from[66,95−97]

$$S(t) = \frac{\Delta\bar{E}(t) - \Delta\bar{E}(\infty)}{\Delta\bar{E}(0) - \Delta\bar{E}(\infty)} \quad (5)$$

where the bar represents the average over all the 480 configurations.

(d). Solvent Free Energy Curves for the Electron Transfer. We focus here on the solvent fluctuations that drive the electron transfer reaction DMA + C314* → $DMA^{+\bullet}$ + $C314^{-\bullet}$. We use the simplified labels D and A for the donor (DMA) and acceptor (C314*) molecules, respectively, and denote by $U_R(\mathbf{r})$ and $U_P(\mathbf{r})$ the total potential energy of the reactant state $\Psi_R = |DA\rangle$ and the product state $\Psi_P = |D^+A^-\rangle$, respectively. As usual, we define the reaction coordinate using the energy gap:[62,98−102]

$$X(\mathbf{r}) = U_P(\mathbf{r}) - U_R(\mathbf{r}) \quad (6)$$

The solvent free energy associated with the solvent fluctuations when the system is in the electronic state $\nu = \Psi_R$ or Ψ_P is given by[62,98,99]

$$A_\nu(x) = -RT\ \ln\langle\delta[X(r) - x]\rangle_\nu \quad (7)$$

The reorganization free energy for the system in state ν is given by the free energy required to change the solvent polarization from the equilibrium value of one state to that of the second state, for example,

$$\lambda_R = A_R(x_P) - A_R(x_R),\ x_\nu = \langle X(\mathbf{r})\rangle_\nu,\ \ \nu = R, P \quad (8)$$

Marcus' assumption of linear response is equivalent to taking $A_R(x)$ and $A_P(x)$ to be paraboli with identical curvatures, which means that $\lambda_R = \lambda_P = \lambda_s$. In recent years, several authors have examined the validity of this assumption[62,100] and proposed approaches to extend Marcus' theory for the case when this assumption does not hold.[102,103]

The activation free energy ΔG^* is obtained from the intersection of $A_R(x)$ and $A_P(x)$, which depends on these functions, as well as on the reaction free energy $\Delta G_{rxn} = \Delta G(R \rightarrow P) = -RT\ \ln\langle e^{-\beta X}\rangle_P$. Because x_R and x_P are typically very different, equilibrium simulations in the states R and P are not sufficient and an umbrella sampling procedure is required. We use the approach developed by King and Warshel[62] by considering a set of intermediate virtual electronic states, ν_m, m = 1, 2, ..., corresponding to the transfer of a fixed fraction of the full electronic charge, and calculate the free energy function for each individual state. These functions are then "stitched" together to reconstruct the desired full functions A_R and A_P.[62,63,104]

The calculations are done by constraining one of the DMA molecules to be at the fixed equilibrium distance from the C314 molecule. This distance is determined so as to minimize the interaction energy between the two molecules at an orientation where the two molecular planes were perpendicular to each other. At this orientation, the overlap between the DMA HOMO and C314 LUMO orbitals calculated by us is most favorable. The additional test calculations where the donor DMA and C314 molecules are each replaced by a point charge inside a spherical cavity held at several fixed distances from each other and using the same methodology are also performed.

All calculations were done at T = 298 K using a combination of the Andersen stochastic method and the Nose-Hoover thermostat.[105] The integration time step is 0.5 fs using the velocity version of the Verlet algorithm.[106] System size effects are minimized by using a molecule centered gradual switching of the forces at the maximum possible switching distance consistent with the boundary conditions, using a switching function with continuous derivatives at the boundaries.

III. RESULTS AND DISCUSSION

1. Neat Interface. A 5 ns constant temperature (T = 298 K) trajectory is used to characterize the neat water/DMA interface by calculating a number of standard properties. We find that these properties are not fundamentally different from those of other interfaces between water and immiscible weakly polar organic liquids. We briefly summarize these results since this is the first theoretical study of this system.

Figure 3 depicts the density profiles of water and DMA along the distance Z normal to the interface. Z = 0 is the location of the Gibbs surface, defined with respect to the water density. It is approximately the plane where the water density is 50% of the bulk value.[107] The surface tension is computed using the Kirkwood-Buff formula generalized to molecular liquids,[108] with the long-range correction of Blokhuis et al.[109] The value obtained at 298 K is $\gamma = 24 \pm 2$ dyn/cm^2. Capillary wave theory predicts that the interface width σ (square root of mean fluctuations) is given by[107] $\sigma = ((k_BT)/(4\pi\gamma)\ \ln(A/\xi_b^2))^{1/2}$, where A is the simulation box surface area and ξ_b is the inverse of an upper limit on the value of the wavenumber of the capillary fluctuations. This is a quantity on the scale of a molecular diameter and typically is set equal to the bulk liquid correlation length (defined as the distance where the bulk liquid radial distribution function's asymptotic value is equal to 1) in the case of the liquid/vapor interface. At the liquid/liquid interface one can use some average of the two bulk liquids, however, the expression for σ given above is not sensitive to the exact choice of ξ_b. Using the computed value of the surface tension and our simulation box surface area, and taking ξ_b = 3.7 Å, we obtain σ = 2.5 Å. The value we obtain from the density profile in Figure 3 is 2.8 Å.

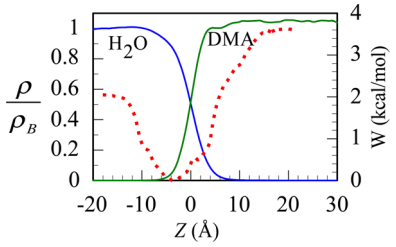

Figure 3. Average (relative to the bulk) density profiles of water and DMA along the surface normal (values depicted on the left axis). The free energy profile of C314 with values given on the right axis is given by the dotted line.

Water molecules' orientation and hydrogen bonding are data that can be compared to experiments once the SFG spectra of the neat system are available. Our results are similar to those of other interfaces between water and weakly polar solvents. The top panel in Figure 4 shows the probability distribution of the angle between the water dipole and the normal to the interface

dx.doi.org/10.1021/jp409541u | J. Phys. Chem. B XXXX, XXX, XXX−XXX

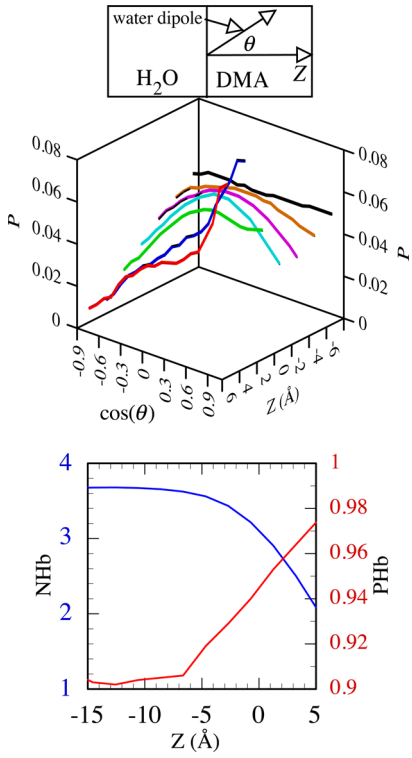

Figure 4. Top panel: The probability distribution of the cosine angle between the water dipole and the normal to the water/DMA interface. Bottom panel: The number of hydrogen bonds per water molecule (blue line, left axis) and the probability of any hydrogen bond being formed (red line, right axis) vs the distance along the interface normal.

in several lamellas parallel to the liquid/liquid interface. As one approaches the Gibbs surface ($Z = 0$) from the water side of the interface ($Z < 0$), the water dipole lies approximately parallel to the interface (broad peak at $\cos\theta \approx 0$). As one crosses the Gibbs surface, the water molecules on the DMA side of the interface have their dipole points on average in the direction toward the DMA. This orientational preference is consistent with having dangling ("free") OH bonds at the interface, which should be observed by the SFG techniques similar to other water-nonpolar solvents like CCl_4.

Complementary information about the structure of the water at the interface can be obtained by examining the hydrogen bonding statistics of water molecules. For our purpose here, two water molecules are defined as hydrogen-bonded if their mutual interaction energy is more negative than 10 kJ/mol.[110−112] However, a geometric criterion[113−115] based on the O−O distance being less than 3.5 Å (the location of the first minimum of the bulk water oxygen−oxygen radial distribution function) with the O−H−O angle deviating by no more than 30° from linearity gives essentially the same results (for a more detailed discussion of hydrogen bond definitions and a systematic approach for developing H-bond criteria using a geometric cutoff, see ref 116). The bottom panel of Figure 4 shows on the left axis the number of hydrogen bonds per water molecule *N*Hb and on the right the ratio of this number to the local coordination number, which gives *P*Hb, the conditional probability for any given hydrogen bond to exist. These are calculated by averaging the statistics of water molecules in lamellas of thickness 2 Å parallel to the interface. In bulk water, each water molecule is hydrogen-bonded by an average of 3.6 hydrogen bonds to other water molecules. Given that the coordination number of water in the bulk is about 4, this shows that the probability for any given hydrogen bond to exist is about 0.9. At the water/DMA interface, the number of hydrogen bonds per water molecule decreases to an average of 2.5 at the Gibbs surface. However, the coordination number also decreases to a value of about 2.6 (reflecting the existence of dangling hydrogen bonds). Thus, the probability that any of the water molecules in the first coordination shell is hydrogen-bonded is a higher value (0.96) at the interface than in the bulk. The same qualitative picture emerges in several water interfacial systems.[117−120]

Turning next to the issue of the interfacial orientation of the DMA molecule, we note that due to its low polarity (dipole moment = 1.7 D) and relatively diffuse charge distribution, the molecule does not experience strong electrostatic anisotropic forces at the interface. The DMA orientation is monitored by computing the probability distribution of the cosine angle between the interface normal and the vector pointing from the nitrogen atom to the para carbon atom of the aromatic ring. The results are shown in Figure 5 as a function of the distance

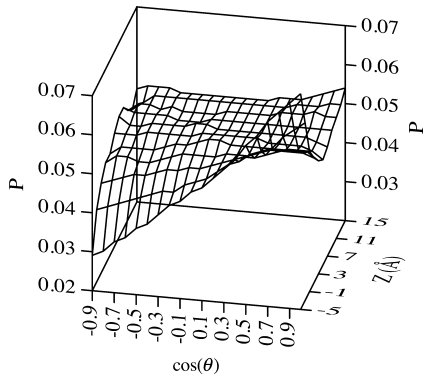

Figure 5. Probability distribution of the cosine angle between the DMA N-pC vector and the normal to the water/DMA interface.

along the interface normal. The distribution is completely random up to just a couple of angstroms from the Gibbs surface on the organic side of the interface. DMA molecules near the Gibbs surface and those that protrude into the aqueous phase are oriented with the amine group pointing toward the water, but the preference is not dramatic: $P(\cos\theta = 1)/P(\cos\theta = -1) \approx 2$. As a result, despite the low polarity of the benzene ring's part of the molecule, the weak orientational preference at the interface does not lead to the creation of an oriented monolayer of DMA molecules (in contrast with the case of the water/octanol interface[121]) and, thus, does not support the supposition that the *neat interface* has a region whose polarity is significantly less than that of the bulk organic phase. Thus, our conclusion is that the experimental observation of low surface polarity must be due to the specific solute−solvent interactions and is not an inherent property of the neat interface. This will be discussed further below.

2. Coumarin Adsorption at the Water/DMA Interface. The 5 ns equilibrium calculations in each 3 Å wide lamella, as explained above, provide a reasonably convergent free energy profile of transporting C314 across the water/DMA interface. This is plotted versus the center of mass of this molecule along the interface normal and is superimposed on the density profiles of the two solvents in Figure 3. The significant relatively deep minimum (observed about 3 Å from the Gibbs

dx.doi.org/10.1021/jp409541u | J. Phys. Chem. B XXXX, XXX, XXX−XXX

surface on the water side of the interface) is consistent with the experimentally observed monolayer formation at the water/DMA interface.

A longer (20 ns) equilibrium trajectory is used in the window centered at the location of the free energy minimum to obtain relatively accurate orientation and rotational dynamics of the C314 at the interface. The top panel of Figure 6 shows the

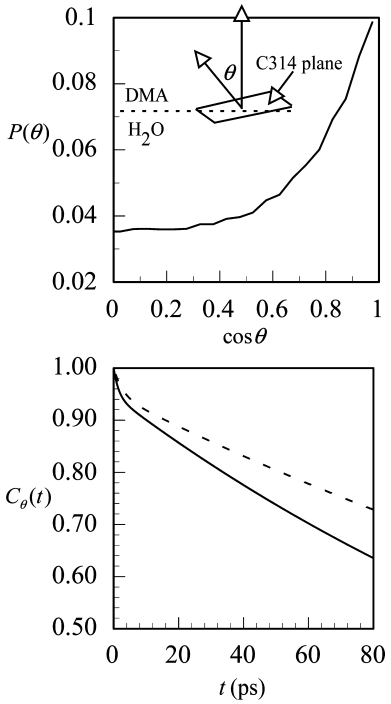

Figure 6. Coumarin 314 at the water/DMA interface. Top: Orientational probability distribution. Bottom: Rotational dynamics with solid blue line depict the reorientation of the vector normal to the C314 plane and dashed red line for the vector along the ground state dipole.

probability distribution of the cosine angle between the normal to the rings plane of C314 and the normal to the interface. There is a clear preference for the rings plane to be parallel to the interface, but the free energy required to tilt the molecule by 90° is only equal to about kT ln(0.1/0.035) ≈ kT per molecule. This effective potential (resulting from the C314-solvents' intermolecular interactions) and the large moment of inertia are responsible for the slow reorientation of the molecule. The reorientation dynamics are computed by following the time correlation function:

$$C_\theta(t) = \frac{\langle \cos\theta(t)\cos\theta(0)\rangle}{\langle \cos^2\theta(t)\rangle} \quad (9)$$

This function is shown in the bottom panel of Figure 6 for the reorientation of the vector normal to the molecule rings plane (solid blue line) and for the reorientation of the vector that lies along the molecule's ground state electric dipole (dashed red line). Each correlation function exhibits a small initial rapid decay corresponding to inertial dynamics (with a time constant of 3–4 ps), followed by a much slower tail representing rotational diffusion. The rotational relaxation times (as determined from a fit of the tail to an exponential) are 280 ± 30 ps and 365 ± 40 ps for the normal vector and for the dipole vector, respectively. A direct experimental probe of the reorientation dynamics of C314 at the water/DMA interface is complicated by the fact that the SFG signal is determined by both the electronic state population and the orientation of C314 and the fact that the time scale of the rotational dynamics of C314 seems to overlap with the dynamics of the back electron transfer reaction.[51] Measurement of the rotational dynamics of C314 at the interface between water and benzonitrile (a liquid with similar structure and viscosity as DMA) in order to separate the back electron transfer from the rotational dynamics of C314 yields a rotation time of 245 ± 20 ps. This is in fair agreement with our calculations.

3. Solvation Dynamics. An important dynamical process which, according to analysis of the experimental data,[37,51] overlaps with the electron transfer is the solvation dynamics of the excited state C314. Thus, it is important to verify that our model potential energy functions provide a reasonable description of this process. The fact that C314 is strongly adsorbed at the interface allows us to calculate the solvation dynamics following excitation of C314 without using a restraining potential to keep it at the interface. The calculations are done as explained in section II, and both the equilibrium correlation function (eq 4) and the nonequilibrium correlation function (eq 5), which is more directly related to experimental observations, are discussed next.

The top panel of Figure 7 shows the nonequilibrium correlation function $S(t)$ following excitation of C314 in bulk

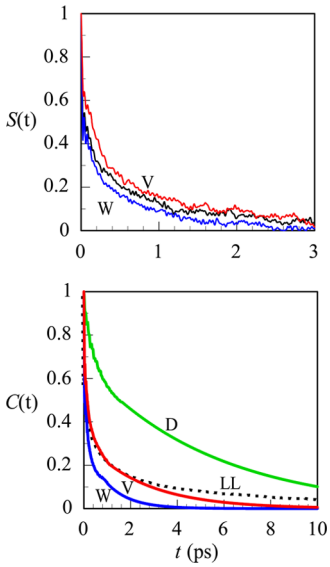

Figure 7. Solvation dynamics of C314 in different environments. Top panel: The nonequilibrium correlation function (eq 5) calculated when the C314 is in bulk water (blue line labeled W), at the water liquid/vapor interface (red line labeled V), and at the water/DMA interface (unlabeled black line). Bottom panel: The equilibrium correlation functions (eq 4) in bulk water (blue line labeled W), water liquid/vapor interface (red line labeled V), at the water/DMA liquid–liquid interface (black dotted line labeled LL), and in bulk DMA (green line labeled D).

water and at the water/DMA interface. We also show the results at the water liquid/vapor interface, since experimental data on this system are also available,[122,123] providing an additional check on our model. Generally, our calculations show that the solvation dynamics take place on the picosecond time scale and are relatively insensitive to the environment. A fit to a biexponential function shows that each dynamic is

dx.doi.org/10.1021/jp409541u | J. Phys. Chem. B XXXX, XXX, XXX–XXX

characterized by a fast, ≈100 fs, component accounting for about 40% of the total relaxation followed by a slower 0.9−1.4 ps tail, with bulk water showing the fastest relaxation (0.9 ps) and the liquid/vapor the slowest (1.4 ps). These are in reasonable agreement with the experimentally measured time constants (2.2 ± 0.3 ps at the liquid/vapor interface,[123] similar to that at the water/DMA interface[51] and 0.9 ps in bulk water[124]). Our calculations at the water liquid/vapor interface are also in reasonable agreement with the calculations reported by Laria and co-workers.[125] The fact that the interface relaxation is closer to that of bulk water reflects the fact that most of the solvation energy at the interface is provided by the water, which is consistent with other computational studies of interfacial solvation dynamics.[66]

The bottom panel of Figure 7 depicts the equilibrium correlation function $C(t)$, as determined from the energy gap fluctuations when the C314 charge distribution is that of the excited state. Under the linear response assumption,[95−97] $C(t) \approx S(t)$. Our calculations show that linear response, while not perfect, is quite accurate in bulk water and a little less so at the liquid/liquid and liquid/vapor interfaces (note the different time scale between the top and bottom graphs). In the bottom panel, we also show the result in bulk DMA. In this case, the equilibrium correlation function decays significantly more slowly (τ = 5.6 ps) due to the significantly slower motion of the solvent molecules.

The solvent contribution ΔE to the energy gap between the excited and ground state coumarin provides a possible explanation of the experimental observation of low surface polarity. In Figure 8, we show the probability distribution

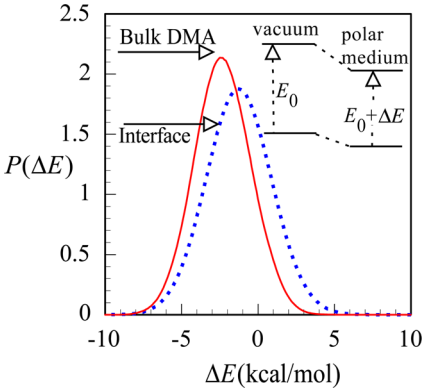

Figure 8. Probability distribution (area normalized) of the solvent contribution to the excited−ground state energy gap of C314 in bulk DMA and at the water/DMA interface. The inset defines the energies involved.

$P(\Delta E)$ for coumarin at the water/DMA interface and in bulk DMA. Ignoring vibrational contributions, these plots essentially give the bulk versus interfacial absorption spectra relative to the gas phase value. The slight red shift when C314 is in bulk DMA relative to the interface is consistent with a lower polarity of the interface, although our calculations suggest a smaller effect than what was observed experimentally. This could be due to the simplified nature of our solute charge distribution, as well as the neglect of the many-body polarizability contribution to the solvation energy of the C314 excited state from the polarizable DMA molecules.[66,126] Nevertheless, these calculations suggest that the low polarity of the interface region is due to the nature of the solvent−solute interactions and not to an inherent property of the neat interface.

4. Electron Transfer. The solvent free energy curves for the reactants state (DMA + C314*) and for the products state ($DMA^{+\bullet}$ + $C314^{-\bullet}$) are shown in Figure 9. As discussed in

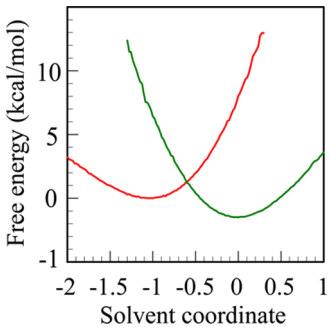

Figure 9. Solvent free energy curves for the reactants state (DMA + C314*, red line) and for the products state ($DMA^{+\bullet}$ + $C314^{-\bullet}$, green line) calculated by direct sampling of the energy gap solvent coordinate. The solvent coordinate values are normalized as explained in the text. The curves are shifted by the value of ΔG_{rxn} estimated independently, as explained in the text.

section II.2(d), these curves are calculated by direct sampling of the ET energy gap coordinate. The equilibrium value of this coordinate when the system is in the reactants or products state is normalized to −1 and 0, respectively. These curves show that the reorganization free energy for this reaction is remarkably small: λ = 1.60 kcal/mol for the reactants state and λ = 1.58 kcal/mol for the products state. The near equality of these two values of λ is consistent with the linear response assumption, namely, that the reorganization free energy be independent of the electronic state.

In order to obtain the activation free energy for the reaction, one requires the reaction free energy ΔG_{rxn}. This can be estimated using the Rehm−Weller equation, which requires excitation energy and redox potentials and assumes spherical ions in a continuum electrostatic model.[127] (As an example for using this approach, see ref 59.) As will be demonstrated below, the assumption of spherical ions in a continuum electrostatic solvent is quite poor here. Within our molecular model, we can determine the reaction free energy using

$$\Delta G_{rxn} = \Delta G(R \rightarrow P) = -RT \ln\langle e^{-\beta X}\rangle_P \quad (10)$$

The energy gap X defined in eq 6 can be written in more detail as follows:

$$X(\mathbf{r}) = U_P(\mathbf{r}) - U_R(\mathbf{r}) = \Delta u_S(\mathbf{r}) + u_{IP} + \delta E_0 \quad (11)$$

where $\Delta u_S(\mathbf{r}) = u_{PS}(\mathbf{r}) - u_{RS}(\mathbf{r})$. The terms u_{PS} and u_{RS} are the total interaction energies between all the solvent molecules (water and DMA molecules, excluding the one DMA molecule selected to be the electron donnor) and the product (P) molecules and reactant (R) molecules, respectively; u_{IP} is the interaction between the ion pairs $DMA^+/C314^-$ held at a fixed separation R (this quantity is estimated to be $-1/\varepsilon R$, with ε being the dielectric constant of the medium in the Rhem-Weller expression); and δE_0 is the gas phase energy difference equal to the difference between the ionization potential of the donor and the electron affinity of the acceptor, minus the energy corresponding to the wavelength where the emission

dx.doi.org/10.1021/jp409541u | J. Phys. Chem. B XXXX, XXX, XXX−XXX

and absorption spectra cross.[59,127] From eqs 10 and 11 we obtain

$$\Delta G_{rxn} = -RT \ln\langle e^{-\beta \Delta u}\rangle_P + u_{IP} + \delta E_0 \quad (12)$$

The direct sampling of the energy gap in the first term on the right side of eq 12 gives for this term the value of −0.3 kcal/mol. Unfortunately, the other two terms are much larger, with opposite signs and uncertainties that are larger than 0.3 kcal/mol but of the same order of magnitude. If we assume $\delta E_0 \approx -u_{IP}$, we find that the activation free energy for the forward reaction is predicted by our model to be only 0.39 kcal/mol. (This is also reflected in the drawing of Figure 9.) Using these values and the estimated τ_L = 0.4 ps for the solvation dynamics time constant, our rate is estimated to be $k_{ET} \approx [(\lambda_s)/(16\pi k_B T)]^{1/2} \times (1/\tau_L) e^{-\Delta G^*/k_B T}$ = 0.3 ps^{-1} compared with the experimental value of 0.07 ± 0.01 ps^{-1}. Our faster rate could be due to slight deviation from adiabaticity (see discussion below), neglect of the intramolecular contribution to the reorganization free energy,[128] as well as uncertainties regarding the potential energy functions and the value of the reaction free energy.

The small value of the reorganization free energy is surprising given the much larger values predicted from a simple point-charge-in-a-spherical-cavity model of each of the two charge transfer centers. The results of these calculations are shown in Figure 10. The full umbrella sampling calculations show that a linear response is only a borderline reasonable approximation (about a 15−20% difference between the values of the product and reactant states' reorganization free energies). The increase in λ as the distance between the two spheres is increased (going from top to bottom panels) is consistent with general ET theory and continuum models.[54,56] The fact that the reorganization free energy at the interface is larger than in the bulk (by about a factor of 2.5) for this simple spherical charge transfer state is also consistent with continuum models[54] and suggests that the polarity of the interface is larger than that of bulk DMA, as was also reflected in the solvation dynamics calculations. We conclude that the significant difference in the reorganization free energy between these two ET models is due to the fact that the local electric field (and the polarity) sensed by the point charge probes at the interface is significantly different than what is sensed by the quite diffuse charge distribution of the DMA and C314 molecules. This is similar to the previously reported examples of the dependence of interfacial polarity on the nature of the molecular probe.[66,129]

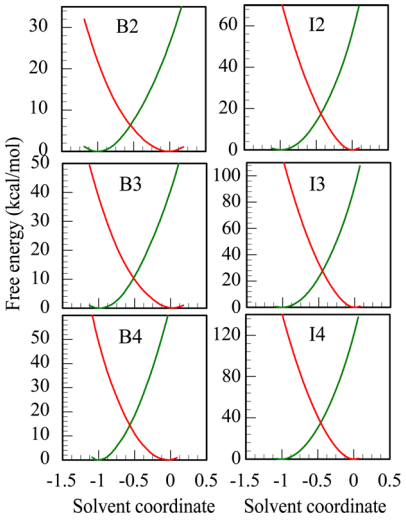

Figure 10. Solvent free energy curves for the reactants state (DA red line) and for the products state (D^+A^-, green line) calculated by umbrella sampling of the energy gap solvent coordinate. The solvent coordinate values are normalized, as explained in the text. The panels on the left and right are for the atomic pair in bulk DMA (labeled B) and at the water/DMA interface (labeled I), respectively. The top, middle, and bottom panels are for the atomic pair to be at a distance of 2, 3, and 4 Å, respectively. Note the different free energy scales of the various panels.

As pointed out in the Introduction, the faster (by a factor of 2) rate at the interface than in bulk DMA was attributed to the lower polarity and thus lower reorganization free energy. Our calculations show that, while the interface polarity (as determined by the shift in the solvent contribution shown in Figure 8) is somewhat smaller than in the bulk, the difference is probably too small to account for the rate enhancement. Indeed, our calculation of the reorganization free energy in bulk DMA (not shown) gives identical results to the calculations at the water/DMA interface. If we repeat the analysis described above for the calculation of the reaction free energy (using the same assumptions), we find that our model predicts that the activation free energy in bulk DMA and at the water/DMA interface are both very small. Thus, this is not likely the reason for the different rates observed experimentally. It is more likely that the slower rate in bulk DMA is due to the slower solvation dynamics. Our calculation of the solvation dynamics in bulk DMA (bottom panel of Figure 7) suggests a surface rate that is a factor of 5.6/0.4 = 14 larger. However, the ET rate enhancement at the interface is likely much less than a factor of 14 due to the fact that there are less favorable C314/DMA contacts at the interface than in the bulk and that the adiabaticity parameter is less than 1 (see next section). Another factor that may affect the measured rate at the interface is possible C314−C314 interaction due to aggregation. From the surface tension measurements, it was concluded that the surface density of C314 is 10^{13} molecules/cm^2.[37] This gives a surface area per molecule of about 1000 Å and thus an average C314−C314 distance of about 31 Å, suggesting that chromophore−chromophore interactions are not a major concern. However, it would be interesting to conduct the ET experiments at different bulk C314 concentrations.

We conclude by examining the conditions under which the reaction can be considered to be in the adiabatic regime at the interface, thus, justifying the use of the above expression for the rate constant. The electronic coupling constant for the ET between excited state C314 and DMA has not been calculated, but calculations on similar coumarin molecules suggest that the coupling is very sensitive to the orientation of the donor/acceptor pair and could be quite large.[49] Here we discuss the following question: Assuming that in bulk DMA the C314 has sufficient opportunity to arrive at the correct orientation so the molecular orbitals achieve sufficient overlap and the electron transfer can be regarded as adiabatic, does the reaction remain adiabatic at the interface? With the aid of unrestricted molecular dynamics simulations of C314 in bulk DMA and at the water/DMA interface, we can provide a partial answer to this question as follows.

We assume that the electronic coupling constant V_{el} introduced in eq 1 varies with the distance R between the two molecules' centers of mass and the angle θ between the two vectors normal to the molecular planes according to

dx.doi.org/10.1021/jp409541u | J. Phys. Chem. B XXXX, XXX, XXX−XXX

$$V_{el} = V_0 e^{-\alpha(R-R_0)}, \quad \alpha = \alpha_0 e^{-\gamma\theta^2} \tag{13}$$

Substituting in the expression for the adiabaticity constant κ (eq 1), we obtain:

$$\kappa = \frac{4\pi V_{el}^2 \tau_L}{\hbar\lambda} = \frac{4\pi V_0^2 e^{2\alpha R_0}\tau_L}{\hbar\lambda} e^{-2\alpha R} \tag{14}$$

Fluctuations in the distance between the ET pair give rise to corresponding fluctuations in the value of κ. The distribution of possible values of κ is given in terms of the DMA/C314 radial distribution function $g(R)$:

$$\rho_\kappa(\kappa)d\kappa = 4\pi\rho_{DMA} R^2 g(R) dR \tag{15}$$

Combining eqs 14 and 15 gives

$$\rho_\kappa(\kappa) = \frac{4\pi\rho_{DMA} R^2 g(R)}{|d\kappa/dR|} = \frac{2\pi\rho_{DMA} R^2 g(R)}{\alpha\kappa} \tag{16}$$

If we take $\alpha = 1$ Å^{-1}, all the other constants in eq 14 except V_0 are known. One can then determine κ versus R, and thus, using eq 16, plot ρ_κ versus κ for different choices of V_0 from the knowledge of $g(R)$ in bulk DMA and at the interface (Figure 11). The results are shown in Figure 12.

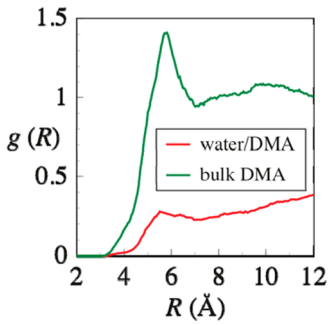

Figure 11. C314*/DMA center of mass radial distribution functions in bulk DMA and at the water/DMA interface.

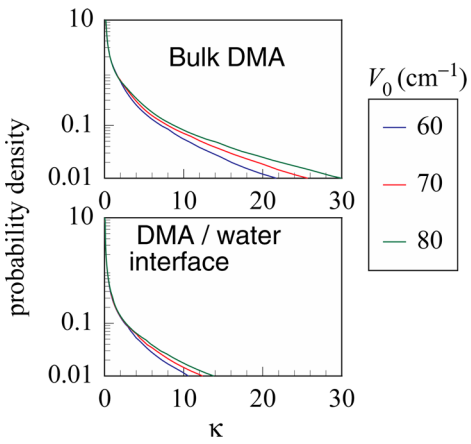

Figure 12. Probability density of the adiabaticity parameter κ (eq 16) for different choices of the electronic coupling constant V_0 for C314 in bulk DMA and at the water/DMA interface.

As expected, the probability for observing a large value of κ decreases with increasing value of κ, and it is also quite sensitive to the value of V_0. If we take $\kappa > 10$ as indicative of an adiabatic ET, there is a significant probability for the ET pair to be at distances that give rise to this value of κ in the bulk. The bottom panel shows that the probability of being in the adiabatic regime at the water/DMA interface is smaller than that in the bulk (due to the significantly fewer DMA/C314 contacts) and thus will likely contribute to reducing the value of the rate constant. However, the probability for the ET to be in the adiabatic regime is not negligible and could be significant if the electronic coupling is large.

IV. CONCLUSIONS

Our detailed molecular dynamic study of a photoinduced electron transfer reaction at a liquid/liquid interface sheds light on several molecular processes that are central to the understanding of this reaction. Our calculations are in general agreement with experimental data on solute rotation, solvation dynamics and the rate of the electron transfer. These calculations demonstrate the importance of molecular-level detail for understanding interfacial phenomena. In particular, a simple representation of the charge transfer centers as point charges in spherical cavities significantly overestimates the reorganization free energy of the electron transfer. Surface structural fluctuations are shown to be important for elucidating solvation dynamics responses. A simple analysis also shows that the adibaticity of interfacial ET reactions is sensitive to local interface structural fluctuations. The rate enhancement at the interface relative to the bulk is likely due to several competing factors: Faster solvation dynamics at the interface will increase the rate, but more intermolecular contact and an adiabaticity parameter closer to 1 in the bulk will counteract this.

■ ASSOCIATED CONTENT

Supporting Information

DMA and Coumarin parameters. This material is available free of charge via the Internet at http://pubs.acs.org.

■ AUTHOR INFORMATION

Notes

The authors declare no competing financial interest.

■ ACKNOWLEDGMENTS

This work has been supported by a grant from the National Science Foundation (CHE-0809164). We thank the reviewers for useful suggestions.

■ REFERENCES

(1) Kharkats, Y. I.; Volkov, A. G. Interfacial Catalysis: Multielectron Reactions at the Liquid−Liquid Interface. *J. Electroanal. Chem.* **1985**, *184*, 435−442.

(2) Girault, H. H.; Schiffrin, D. J. Electrochemistry of Liquid−Liquid Interfaces. In *Electroanalytical Chemistry*; Bard, A. J., Ed.; Dekker: New York, 1989; p 1.

(3) Schmickler, W. *Interfacial Electrochemistry*; Oxford University Press: Oxford, 1996.

(4) Bard, A. J.; Mirkin, M. V. *Scanning Electrochemical Microscope*; Marcel Dekker: New York, 2001.

(5) Osakai, T.; Hotta, H., Electron Transfer at Liquid/Liquid Interfaces. In *Interfacial Nanochemistry: Molecular Science and Engineering at Liquid-Liquid Interfaces*; Watarai, H., Teramae, N., Sawada, T., Eds. Kluwer Academic/ Plenum: New York, 2005; pp 171−188.

(6) Dryfe, R. A. W. The Electrified Liquid−Liquid Interface. *Adv. Chem. Phys.* **2009**, *141*, 153−215.

(7) Samec, Z. Dynamic Electrochemistry at the Interface between Two Immiscible Electrolytes. *Electrochim. Acta* **2012**, *84*, 21−28.

(8) Fermin, D. J.; Duong, H. D.; Ding, Z. F.; Brevet, P. F.; Girault, H. H. Solar Energy Conversion Using Dye-Sensitised Liquid Vertical Bar Liquid Interfaces. *Electrochem. Commun.* **1999**, *1*, 29−32.
(9) Lahtinen, R.; Fermin, D. J.; Kontturi, K.; Girault, H. H. Artificial Photosynthesis at Liquid Vertical Bar Liquid Interfaces: Photoreduction of Benzoquinone by Water Soluble Porphyrin Species. *J. Electroanal. Chem.* **2000**, *483*, 81−87.
(10) Starks, C. M.; Liotta, C. L.; Halpern, M. *Phase Transfer Catalysis*; Chapman and Hall: New York, 1994.
(11) Campbell, C. J.; Rusling, J. F. Electrochemical Phase Transfer Catalysis in Microemulsions: Carbene Formation. *Langmuir* **1999**, *15*, 7416−7417.
(12) Makosza, M. Phase Transfer Catalysis. A General Green Methodology in Organic Synthesis. *Pure Appl. Chem.* **2000**, *72*, 1399−1403.
(13) Barbara, P. F.; Olson, E. J. J. Experimental Electron Transfer Kinetics in a DNA Environment. *Adv. Chem. Phys.* **1999**, *107*, 647−676.
(14) Volkov, A. G.; Deamer, D. W. *Liquid−Liquid Interfaces*; CRC Press: Boca Raton, FL, 1996.
(15) Wei, C.; Bard, A. J.; Mirkin, M. V. Scanning Electrochemical Microscopy 0.31. Application of Secm to the Study of Charge-Transfer Processes at the Liquid−Liquid Interface. *J. Phys. Chem.* **1995**, *99*, 16033−16042.
(16) Solomon, T.; Bard, A. J. Reverse (Uphill) Electron Transfer at the Liquid/Liquid Interface. *J. Phys. Chem.* **1995**, *99*, 17487−17489.
(17) Tsionsky, M.; Bard, A. J.; Mirkin, M. V. Scanning Electrochemical Microscopy 0.34. Potential Dependence of the Electron-Transfer Rate and Film Formation at the Liquid/Liquid Interface. *J. Phys. Chem.* **1996**, *100*, 17881−17888.
(18) Liu, B.; Mirkin, M. V. Potential-Independent Electron Transfer Rate at the Liquid/Liquid Interface. *J. Am. Chem. Soc.* **1999**, *121*, 8352−8355.
(19) Ding, Z.; Quinn, B. M.; Bard, A. J. Kinetics of Heterogeneous Electron Transfer at Liquid/Liquid Interfaces as Studied by Secm. *J. Phys. Chem. B* **2001**, *105*, 6367−6374.
(20) Liu, B.; Mirkin, M. V. Electron Transfer at Liquid/Liquid Interfaces. The Effects of Ionic Adsorption, Electrolyte Concentration, and Spacer Length on the Reaction Rate. *J. Phys. Chem. B* **2002**, *106*, 3933−3940.
(21) Zhang, J.; Unwin, P. R. Microelectrochemical Measurements of Electron Transfer Rates at the Interface between Two Immiscible Electrolyte Solutions: Potential Dependence of the Ferro/Ferricyanide-7,7,8,8-Tetracyanoquinodimethane (TCNQ)/$TCNQ^{\bullet-}$ System. *Phys. Chem. Chem. Phys.* **2002**, *4*, 3820−3827.
(22) Bai, Y. M.; Sun, P.; Zhang, M. Q.; Gao, Z.; Yang, Z. Y.; Shao, Y. H. Effects of Solution Viscosity on Heterogeneous Electron Transfer across a Liquid/Liquid Interface. *Electrochim. Acta* **2003**, *48*, 3447−3453.
(23) Georganopoulou, D. G.; Mirkin, M. V.; Murray, R. W. SECM Measurement of the Fast Electron Transfer Dynamics between Au-38(1+) Nanoparticles and Aqueous Redox Species at a Liquid/Liquid Interface. *Nano Lett.* **2004**, *4*, 1763−1767.
(24) Zhang, M. Q.; Liu, H.; Hu, H.; Xie, S. B.; Jing, P.; Kou, Y.; Shao, Y. H. Studies of Electron Transfer Reactions at the Interface between Room-Temperature Ionic Liquid+1,2-Dichloroethane Solutions and Water by Scanning Electrochemical Microscopy. *Chem. Res. Chin. Univ.* **2006**, *27*, 1355−1359.
(25) Li, F.; Whitworth, A. L.; Unwin, P. R. Measurement of Rapid Electron Transfer across a Liquid/Liquid Interface from 7,7,8,8-Tetracyanoquinodimethane Radical Anion in 1,2-Dichloroethane to Aqueous Tris(2,2-bipyridyl)-Ruthenium (III). *J. Electroanal. Chem.* **2007**, *602*, 70−76.
(26) Laforge, F. O.; Sun, P.; Mirkin, M. V. Physicochemical Applications of Scanning Electrochemical Microscopy. *Adv. Chem. Phys.* **2008**, *139*, 177−244.
(27) Shi, C.; Anson, F. C. Electron Transfer between Reactants Located on Opposite Sides of Liquid/Liquid Interfaces. *J. Phys. Chem. B* **1999**, *103*, 6283−6289.
(28) Shi, C.; Anson, F. C. Rates of Electron-Transfer across Liquid/Liquid Interfaces. Effects of Changes in Driving Force and Reaction Reversibility. *J. Phys. Chem. B* **2001**, *105*, 8963−8969.
(29) Kott, K. L.; Higgins, D. A.; McMahon, R. J.; Corn, R. M. Observation of Photoinduced Electron Transfer at a Liquid−Liquid Interface by Optical Second Harmonic Generation. *J. Am. Chem. Soc.* **1993**, *115*, 5342.
(30) Dryfe, R. A. W.; Ding, Z.; Wellington, R. G.; Brevet, P. F.; Kuznetzov, A. M.; Girault, H. H. Time-Resolved Laser-Induced Fluorescence Study of Photoinduced Electron Transfer at the Water/1,2-Dichloroethane Interface. *J. Phys. Chem. A* **1997**, *101*, 2519−2524.
(31) Weidemaier, K.; Tavernier, H. L.; Fayer, M. D. Photoinduced Electron Transfer on the Surfaces of Micelles. *J. Phys. Chem. B* **1997**, *101*, 9352−9361.
(32) Fermin, D. J.; Ding, Z.; Duong, H. D.; Brevet, P.-F.; Girault, H. H. Photoinduced Electron Transfer at Liquid/Liquid Interfaces. 1. Photocurrent Measurements Associated with Heterogeneous Quenching of Zinc Porphyrins. *J. Phys. Chem. B* **1998**, *102*, 10334−10341.
(33) Fermin, D. J.; Duong, H. D.; Ding, Z.; Brevet, P.-F.; Girault, H. H. Photoinduced Electron Transfer at Liquid/Liquid Interfaces. Part III. Photoelectrochemical Responses Involving Porphyrin Ion Pairs. *J. Am. Chem. Soc.* **1999**, *121*, 10203−10210.
(34) Jensen, H.; Kakkassery, J. J.; Nagatani, H.; Fermin, D. J.; Girault, H. H. Photoinduced Electron Transfer at Liquid/Liquid Interfaces. Part IV. Orientation and Reactivity of Zinc Tetra(4-carboxyphenyl) Porphyrin Self-Assembled at the Water−1,2-Dichloroethane Junction. *J. Am. Chem. Soc.* **2000**, *122*, 10943−10948.
(35) Eugster, N.; Fermin, D. J.; Girault, H. H. Photoinduced Electron Transfer at Liquid/Liquid Interfaces. Part VI. On the Thermodynamic Driving Force Dependence of the Phenomenological Electron-Transfer Rate Constant. *J. Phys. Chem. B* **2002**, *106*, 3428−3433.
(36) Eugster, N.; Fermin, D. J.; Girault, H. H. Photoinduced Electron Transfer at LiquidlLiquid Interfaces: Dynamics of the Heterogeneous Photoreduction of Quinones by Self-Assembled Porphyrin Ion Pairs. *J. Am. Chem. Soc.* **2003**, *125*, 4862−4869.
(37) McArthur, E. A.; Eisenthal, K. B. Ultrafast Excited-State Electron Transfer at an Organic Liquid/Aqueous Interface. *J. Am. Chem. Soc.* **2006**, *128*, 1068−1069.
(38) Ghosh, S.; Sahu, K.; Mondal, S. K.; Sen, P.; Bhattacharyya, K. A Femtosecond Study of Photoinduced Electron Transfer from Dimethylaniline to Coumarin Dyes in a Cetyltrimethylammonium Bromide Micelle. *J. Chem. Phys.* **2006**, *125*, 054509−15.
(39) Ghosh, S.; Mondal, S. K.; Sahu, K.; Bhattacharyya, K. Ultrafast Electron Transfer in a Nanocavity. Dimethylaniline to Coumarin Dyes in Hydroxypropyl γ-Cyclodextrin. *J. Phys. Chem. A* **2006**, *110*, 13139−13144.
(40) Ghosh, S.; Mondal, S. K.; Sahu, K.; Bhattacharyya, K. Ultrafast Photoinduced Electron Transfer from Dimethylaniline to Coumarin Dyes in Sodium Dodecyl Sulfate and Triton X-100 Micelles. *J. Chem. Phys.* **2007**, *126*, 204708−18.
(41) Chakraborty, A.; Chakrabarty, D.; Hazra, P.; Seth, D.; Sarkar, N. Photoinduced Intermolecular Electron Transfer between Coumarin Dyes and Electron Donating Solvents in Cetyltrimethylammonium Bromide (CTAB) Micelles: Evidence for Marcus Inverted Region. *Chem. Phys. Lett.* **2003**, *382*, 508−517.
(42) Chakraborty, A.; Seth, D.; Chakrabarty, D.; Hazra, P.; Sarkar, N. Photoinduced Electron Transfer from Dimethyl Aniline to Coumarin Dyes in Reverse Micelles. *Chem. Phys. Lett.* **2005**, *405*, 18−25.
(43) Chakraborty, A.; Seth, D.; Setua, P.; Sarkar, N. Photoinduced Electron Transfer in a Protein−Surfactant Complex: Probing the Interaction of Sds with Bsa. *J. Phys. Chem. B* **2006**, *110*, 16607−16617.
(44) Chakraborty, A.; Seth, D.; Setua, P.; Sarkar, N. Photoinduced Electron Transfer from *N*,*N*-Dimethylaniline to 7-Amino Coumarins in Protein-Surfactant Complex: Slowing Down of Electron Transfer Dynamics Compared to Micelles. *J. Chem. Phys.* **2006**, *124*, 074512−21.
(45) Tsionsky, M.; Bard, A. J.; Mirkin, M. V. Long-Range Electron Transfer through a Lipid Monolayer at the Liquid/Liquid Interface. *J. Am. Chem. Soc.* **1997**, *119*, 10785−10792.

(46) Zu, Y. B.; Fan, F. R. F.; Bard, A. J. Inverted Region Electron Transfer Demonstrated by Electrogenerated Chemiluminescence at the Liquid/Liquid Interface. *J. Phys. Chem. B* **1999**, *103*, 6272−6276.
(47) Jensen, H.; Fermin, D. J.; Girault, H. H. Photoinduced Electron Transfer at Liquid/Liquid Interfaces. Part V. Organisation of Water-Soluble Chlorophyll at the Water/1,2-Dichloroethane Interface. *Phys. Chem. Chem. Phys.* **2001**, *3*, 2503−2508.
(48) Yoshihara, K. Ultrafast Intermolecular Electron Transfer in Solution. *Adv. Chem. Phys.* **1999**, *107*, 371−402.
(49) Castner, E. W.; Kennedy, D.; Cave, R. J. Solvent as Electron Donor: Donor/Acceptor Electronic Coupling Is a Dynamical Variable. *J. Phys. Chem. A* **2000**, *104*, 2869−2885.
(50) Saik, V. O.; Goun, A. A.; Fayer, M. D. Photoinduced Electron Transfer and Geminate Recombination for Photoexcited Acceptors in a Pure Donor Solvent. *J. Chem. Phys.* **2004**, *120*, 9601−9611.
(51) Rao, Y.; Xu, M.; Jockusch, S.; Turro, N. J.; Eisenthal, K. B. Dynamics of Excited State Electron Transfer at a Liquid Interface Using Time-Resolved Sum Frequency Generation. *Chem. Phys. Lett.* **2012**, *544*, 1−6.
(52) Chakraborty, A.; Seth, D.; Chakrabarty, D.; Sarkar, N. Photoinduced Intermolecular Electron Transfer from Dimethyl Aniline to 7-Amino Coumarin Dyes in the Surface of β-Cyclodextrin. *Spectrochim Acta A* **2006**, *64*, 801−808.
(53) Marcus, R. A. Reorganization Free Energy for Electron Transfers at Liquid−Liquid and Dielectric Semiconductor−Liquid Interfaces. *J. Phys. Chem.* **1990**, *94*, 1050−1055.
(54) Benjamin, I.; Kharkats, Y. I. Reorganization Free Energy for Electron Transfer Reactions at Liquid/Liquid Interfaces. *Electrochim. Acta* **1998**, *44*, 133−138.
(55) Marcus, R. A. Theory of Electron-Transfer Rates Across Liquid−Liquid Interfaces. *J. Phys. Chem.* **1990**, *94*, 4152−4155.
(56) Marcus, R. A. Theory of Electron-Transfer Rates Across Liquid−Liquid Interfaces. 2. Relationships and Application. *J. Phys. Chem.* **1991**, *95*, 2010−2013.
(57) Lewis, N. S. An Analysis of Charge Transfer Rate Constants for Semiconductor/Liquid Interfaces. *Annu. Rev. Phys. Chem.* **1991**, *42*, 543−580.
(58) Smith, B. B.; Halley, J. W.; Nozik, A. J. On the Marcus Model of Electron Transfer at Immiscible Liquid Interfaces and Its Application to the Semiconductor Liquid Interface. *Chem. Phys.* **1996**, *205*, 245−267.
(59) Tavernier, H. L.; Barzykin, A. V.; Tachiya, M.; Fayer, M. D. Solvent Reorganization Energy and Free Energy Change for Donor/Acceptor Electron Transfer at Micelle Surfaces: Theory and Experiment. *J. Phys. Chem. B* **1998**, *102*, 6078−6088.
(60) Harinipriya, S.; Sangaranarayanan, M. V. Analysis of Electron Transfer Processes across Liquid/Liquid Interfaces: Estimation of the Equilibrium Free Energy of Activation. *J. Phys. Chem. B* **2004**, *108*, 1660−1666.
(61) Harinipriya, S.; Sangaranarayanan, M. V. Analysis of Electron Transfer Processes across Liquid/Liquid Interfaces: Estimation of Free Energy of Activation Using Diffuse Boundary Model. *Langmuir* **2006**, *22*, 1347−1355.
(62) King, G.; Warshel, A. Investigation of the Free Energy Functions for Electron Transfer Reactions. *J. Chem. Phys.* **1990**, *93*, 8682−8692.
(63) Benjamin, I. Molecular Dynamics Study of the Free Energy Functions for Electron Transfer Reactions at the Liquid−Liquid Interface. *J. Phys. Chem.* **1991**, *95*, 6675−6683.
(64) Benjamin, I. A Molecular Model for an Electron Transfer Reaction at the Water/1,2-Dichloroethane Interface. In *Structure and Reactivity in Aqueous Solution*, ACS Symposium Series 568; Cramer, C. J., Truhlar, D. G., Eds.; American Chemical Society: Washington, D.C., 1994; p 409.
(65) Wang, H. F.; Borguet, E.; Eisenthal, K. B. Generalized Interface Polarity Scale Based on Second Harmonic Spectroscopy. *J. Phys. Chem. B* **1998**, *102*, 4927−4932.
(66) Benjamin, I. Static and Dynamic Electronic Spectroscopy at Liquid Interfaces. *Chem. Rev.* **2006**, *106*, 1212−1233.
(67) Zusman, L. D. Outer-Sphere Electron Transfer in Polar Solvents. *Chem. Phys.* **1980**, *49*, 295−304.
(68) Sumi, H.; Marcus, R. A. Dynamical Effects in Electron Transfer Reactions. *J. Chem. Phys.* **1986**, *84*, 4894−4914.
(69) Onuchic, J. N. Effect of Friction on Electron Transfer: The Two Reaction Coordinate Case. *J. Chem. Phys.* **1987**, *86*, 3925−3943.
(70) Rips, I.; Jortner, J. Dynamic Solvent Effects on Outer-Sphere Electron Transfer. *J. Chem. Phys.* **1987**, *87*, 2090−2104.
(71) Lakowicz, J. R. *Principles of Fluorescence Spectroscopy*; Springer: New York, 2010.
(72) Steel, W. H.; Walker, R. A. Measuring Dipolar Width across Liquid−Liquid Interfaces with "Molecular Rulers". *Nature* **2003**, *424*, 296−299.
(73) Schlossman, M. L. Liquid−Liquid Interfaces: Studied by X-Ray and Neutron Scattering. *Curr. Opin. Colloid Interface Sci.* **2002**, *7*, 235−243.
(74) Smit, B. Molecular Dynamics Simulation of Amphiphilic Molecules at a Liquid−Liquid Interface. *Phys. Rev. A* **1988**, *37*, 3431−3433.
(75) Benjamin, I. Chemical Reactions and Solvation at Liquid Interfaces: A Microscopic Perspective. *Chem. Rev.* **1996**, *96*, 1449−1476.
(76) Chang, T. M.; Dang, L. X. Molecular Dynamics Simulations of CCl_4−H_2O Liquid−Liquid Interface with Polarizable Potential Models. *J. Chem. Phys.* **1996**, *104*, 6772−6783.
(77) Senapati, S.; Berkowitz, M. L. Computer Simulation Study of the Interface Width of the Liquid/Liquid Interface. *Phys. Rev. Lett.* **2001**, *87*, 176101−4.
(78) Benjamin, I. Mechanism and Dynamics of Ion Transfer across a Liquid−Liquid Interface. *Science* **1993**, *261*, 1558−1560.
(79) Lauterbach, M.; Engler, E.; Muzet, N.; Troxler, L.; Wipff, G. Migration of Ionophores and Salts through a Water−Chloroform Liquid−Liquid Interface: Molecular Dynamics Potential of Mean Force Investigations. *J. Phys. Chem. B* **1998**, *102*, 245−256.
(80) Dang, L. X. Computer Simulation Studies of Ion Transport across a Liquid/Liquid Interface. *J. Phys. Chem. B* **1999**, *103*, 8195−8200.
(81) Wang, H.; Borguet, E.; Eisenthal, K. B. Polarity of Liquid Interfaces by Second Harmonic Generation Spectroscopy. *J. Phys. Chem. A* **1997**, *101*, 713−718.
(82) Steel, W. H.; Beildeck, C. L.; Walker, R. A. Solvent Polarity across Strongly Associating Interfaces. *J. Phys. Chem. B* **2004**, *108*, 16107−16116.
(83) Michael, D.; Benjamin, I. Molecular Dynamics Computer Simulations of Solvation Dynamics at Liquid/Liquid Interfaces. *J. Chem. Phys.* **2001**, *114*, 2817−2824.
(84) Rizzo, R. C.; Jorgensen, W. L. OPLS All-Atom Model for Amines: Resolution of the Amine Hydration Problem. *J. Am. Chem. Soc.* **1999**, *121*, 4827−4836.
(85) Kuchitsu, K.; Morino, Y. Estimation of Anharmonic Potential Constants. II. Bent XY_2 Molecules. *Bull. Chem. Soc. Jpn.* **1965**, *38*, 814−824.
(86) Hansen, J.-P.; McDonald, I. R. *Theory of Simple Liquids*, 2nd ed.; Academic: London, 1986; p 179.
(87) Berendses, H. J. C.; Postma, J. P. M.; van Gunsteren, W. F.; Hermans, J. In *Intermolecular Forces*; Pullman, B., Ed.; D. Reidel: Dordrecht, 1981; p 331.
(88) Pantano, D. A.; Laria, D. Molecular Dynamics Study of Solvation of Coumarin-314 at the Water/Air Interface. *J. Phys. Chem. B* **2003**, *107*, 2971−2977.
(89) Frisch, M. J.; et al. *Gaussian 09*; Gaussian, Inc.: Wallingford, CT, 2009.
(90) Schwabe, T.; Grimme, S. Double-Hybrid Density Functionals with Long-Range Dispersion Corrections: Higher Accuracy and Extended Applicability. *Phys. Chem. Chem. Phys.* **2007**, *9*, 3397−3406.
(91) Breneman, C. M.; Wiberg, K. B. Determining Atom-Centered Monopoles from Molecular Electrostatic Potentials - the Need for High Sampling Density in Formamide Conformational Analysis. *J. Comput. Chem.* **1990**, *11*, 361−373.

(92) Pohorille, A.; Wilson, M. A. Molecular Structure of Aqueous Interfaces. *J. Mol. Struct.: THEOCHEM* **1993**, *103*, 271−298.
(93) Kumar, S.; Rosenberg, J. M.; Bouzida, D.; Swendsen, R. H.; Kollman, P. A. Multidimensional Free-Energy Calculations Using the Weighted Histogram Analysis Method. *J. Comput. Chem.* **1995**, *16*, 1339−1350.
(94) Kastner, J. Umbrella Sampling. *Wires Comput. Mol. Sci.* **2011**, *1*, 932−942.
(95) Chandler, D. *Introduction to Modern Statistical Mechanics*; Oxford University Press: Oxford, 1987.
(96) Carter, E. A.; Hynes, J. T. Solvation Dynamics for an Ion Pair in a Polar Solvent: Time Dependent Fluorescence and Photochemical Charge Transfer. *J. Chem. Phys.* **1991**, *94*, 5961−5979.
(97) Stephens, M. D.; Saven, J. G.; Skinner, J. L. Molecular Theory of Electronic Spectroscopy in Nonpolar Fluids: Ultrafast Solvation Dynamics and Absorption and Emission Line Shapes. *J. Chem. Phys.* **1997**, *106*, 2129−2144.
(98) Hwang, J. K.; Warshel, A. Microscopic Examination of Free-Energy Relationships for Electron Transfer in Polar Solvents. *J. Am. Chem. Soc.* **1987**, *109*, 715−720.
(99) Kuharski, R. A.; Bader, J. S.; Chandler, D.; Sprik, M.; Klein, M. L.; Impey, R. W. Molecular Model for Aqueous Ferrous−Ferric Electron Transfer. *J. Chem. Phys.* **1988**, *89*, 3248−3257.
(100) Carter, E. A.; Hynes, J. T. Solute-Dependent Solvent Force Constants for Ion Pairs and Neutral Pairs in Polar Solvent. *J. Phys. Chem.* **1989**, *93*, 2184−2187.
(101) Rasaiah, J. C.; Zhu, J. J. Reaction Coordinates for Electron Transfer Reactions. *J. Chem. Phys.* **2008**, *129*, 214503.
(102) Vuilleumier, R.; Tay, K. A.; Jeanmairet, G.; Borgis, D.; Boutin, A. Extension of Marcus Picture for Electron Transfer Reactions with Large Solvation Changes. *J. Am. Chem. Soc.* **2012**, *134*, 2067−2074.
(103) Matyushov, D. V.; Voth, G. A. Modeling the Free Energy Surfaces of Electron Transfer in Condensed Phases. *J. Chem. Phys.* **2000**, *113*, 5413−5424.
(104) Tachiya, M. Relation between the Electron-Transfer Rate and the Free Energy Change of Reaction. *J. Phys. Chem.* **1989**, *93*, 7050−7052.
(105) Nosé, S. Constant-Temperature Molecular Dynamics. *J. Phys.: Condens. Matter* **1991**, *2*, SA115−SA119.
(106) Allen, M. P.; Tildesley, D. J. *Computer Simulation of Liquids*; Clarendon: Oxford, 1987.
(107) Rowlinson, J. S.; Widom, B. *Molecular Theory of Capillarity*; Clarendon: Oxford, 1982.
(108) Linse, P. Monte Carlo Simulation of Liquid−Liquid Benzene−Water Interface. *J. Chem. Phys.* **1987**, *86*, 4177−4187.
(109) Blokhuis, E. M.; Bedeaux, D.; Holcomb, C. D. Tail Corrections to the Surface Tension of a Lennard-Jones Liquid−Vapour Interface. *Mol. Phys.* **1995**, *85*, 665−669.
(110) Jorgensen, W. L. Monte-Carlo Results for Hydrogen-Bond Distributions in Liquid Water. *Chem. Phys. Lett.* **1980**, *70*, 326−329.
(111) Matsumoto, M.; Ohmine, I. A New Approach to the Dynamics of Hydrogen Bond Network in Liquid Water. *J. Chem. Phys.* **1996**, *104*, 2705−2712.
(112) Starr, F. W.; Nielsen, J. K.; Stanley, H. E. Fast and Slow Dynamics of Hydrogen Bonds in Liquid Water. *Phys. Rev. Lett.* **1999**, *82*, 2294−2297.
(113) Sceats, M. G.; Rice, S. A. The Water−Water Pair Potential near the Hydrogen-Bonded Equilibrium Configuration. *J. Chem. Phys.* **1980**, *72*, 3236−3247.
(114) Mezei, M.; Beveridge, D. L. Theoretical Studies of Hydrogen Bonding in Liquid Water and Dilute Aqueous Solutions. *J. Chem. Phys.* **1981**, *74*, 622−632.
(115) Luzar, A.; Chandler, D. Hydrogen-Bond Kinetics in Liquid Water. *Nature* **1996**, *379*, 55−57.
(116) Kumar, R.; Schmidt, J. R.; Skinner, J. L. Hydrogen Bonding Definitions and Dynamics in Liquid Water. *J. Chem. Phys.* **2007**, *126*, 204107−1−204107−12.
(117) Benjamin, I. Theoretical Study of the Water/1,2-Dichloroethane Interface: Structure, Dynamics and Conformational Equilibria at the Liquid−Liquid Interface. *J. Chem. Phys.* **1992**, *97*, 1432−1445.
(118) Michael, D.; Benjamin, I. Solute Orientational Dynamics and Surface Roughness of Water/Hydrocarbon Interfaces. *J. Phys. Chem.* **1995**, *99*, 1530−1536.
(119) Michael, D.; Benjamin, I. Molecular Dynamics Simulation of the Water/Nitrobenzene Interface. *J. Electroanal. Chem.* **1998**, *450*, 335−345.
(120) Cordeiro, M. N. D. S. Interfacial Tension Behaviour of Water/Hydrocarbon Liquid-Liquid Interfaces: A Molecular Dynamics Simulation. *Mol. Simul.* **2003**, *29*, 817−827.
(121) Benjamin, I. Polarity of the Water/Octanol Interface. *Chem. Phys. Lett.* **2004**, *393*, 453−456.
(122) Benderskii, A. V.; Eisenthal, K. B. Dynamical Time Scales of Aqueous Solvation at Negatively Charged Lipid/Water Interface. *J. Phys. Chem. A* **2002**, *106*, 7482−7490.
(123) Rao, Y.; Turro, N. J.; Eisenthal, K. B. Solvation Dynamics at the Air/Water Interface with Time-Resolved Sum-Frequency Generation. *J. Phys. Chem. C* **2010**, *114*, 17703−17708.
(124) Zimdars, D.; Dadap, J. I.; Eisenthal, K. B.; Heinz, T. F. Femtosecond Dynamics of Solvation at the Air/Water Interface. *Chem. Phys. Lett.* **1999**, *301*, 112−120.
(125) Pantano, D. A.; Sonoda, M. T.; Skaf, M. S.; Laria, D. Solvation of Coumarin 314 at Water/Air Interfaces Aontaining Anionic Surfactants. I. Low Coverage. *J. Phys. Chem. B* **2005**, *109*, 7365−7372.
(126) Michael, D.; Benjamin, I. Structure, Dynamics, and Electronic Spectrum of *N*,*N*′-Diethyl-*p*-nitroaniline at Water Interfaces. A Molecular Dynamics Study. *J. Phys. Chem. B* **1998**, *102*, 5145−5151.
(127) Rehm, D.; Weller, A. Kinetics of Fluorescence Quenching by Electron and H-Atom Transfer. *Isr. J. Chem.* **1970**, *8*, 259−271.
(128) Scherer, P. O. J. Intramolecular Reorganization of the Electron Donnor *N*,*N*-Dimethylaniline. *J. Phys. Chem. A* **2003**, *17*, 8327−8329.
(129) Steel, W. H.; Walker, R. A. Solvent Polarity at an Aqueous/Alkane Interface: The Effect of Solute Identity. *J. Am. Chem. Soc.* **2003**, *125*, 1132−1133.